

Comparison of two different approaches for computing the gravitational effect of a tesseroid

ANNA MARIA MAROTTA¹, KURT SEITZ², RICCARDO BARZAGHI³, THOMAS GROMBEIN²
AND BERNHARD HECK²

- 1 Department of Earth Sciences ‘Ardito Desio’, University of Milano, L. Cicognara 7, Milano, I-20129 Italy (anna.maría.marotta@unimi.it)
- 2 Geodetic Institute, Karlsruhe Institute of Technology (KIT), Englerstr. 7, Karlsruhe, D-76128 Germany (kurt.seitz@kit.edu)
- 3 DICA, Politecnico di Milano, Piazza Leonardo da Vinci 32, Milano, I-20133 Italy (riccardo.barzaghi@polimi.it)

Received: August 3, 2018; Revised: January 2, 2019; Accepted: March 28, 2019

ABSTRACT

Forward modelling in the space domain is a very important task in geodesy and other geosciences. From topographical or isostatic information in the form of digital terrain model (DTM) and density model, the effects of these parameters or their derivatives on the gravity potential can be evaluated for different applications. In most cases, height or height-layer models are in use, which are gridded with respect to spherical coordinates. This holds for global as well as regional or even local applications. The definition of the spherical gridlines leads immediately to the spherical volume element, that is, the tesseroid. Only in the specific case that the observation point is located on the symmetry axis of the spherical coordinate system does the Newton integral have a closed analytical solution. More specifically, the effect of a tesseroid can be determined by evaluating the analytical solution of a segment of a spherical zonal band. To apply this aspect in practice, the DTM must be transformed into the local spherical azimuthal system of the observation point (UNIPOL approach). In the general case, the Newton integral can be solved, for example, using a Taylor series expansion of the integral kernel and a subsequently applied term-wise integration (GIK approach). Within this contribution, the two fundamentally different tesseroid approaches, namely, the GIK and the UNIPOL approach are compared. This comparison is performed, in particular, with regard to the required computational time and the approximation error under different test scenarios. The numerical studies show that both approaches are equivalent in terms of accuracy for both the gravitational potential and gravity; however, the UNIPOL approach is more time consuming because, for each observation point, the whole DTM must be transformed. Small numerical differences exist between the compared approaches for special constellations regarding the source point and the observation point.

Keywords: tesseroid, gravity forward modelling, Newton integral

1. INTRODUCTION

In many geodetic and geophysical computations, the gravitational effect of the topographic layer plays a key role, for example, in the estimation of intra-crustal structures based on Bouguer anomalies, which are obtained using the gravity data measured on the Earth's surface by removing the topographic effect. Since the computation of this component is crucial, intensive research has been carried out to refine the modelling of the gravitational effect of the topography. In recent years, several methods have been proposed to improve the modelling of this effect in spherical approximation. Particularly, approaches aiming at estimating the gravitational terrain effect based on tesseroid geometry in spherical approximation have been formulated. The relevant studies include those by Heck and Seitz (2007), Grombein et al. (2013), Uieda et al. (2015), Marotta and Barzaghi (2017) and Lin and Denker (2019). In Heck and Seitz (2007), the computation of the potential and gravitational effects of a tesseroid was performed using the Taylor expansion of the related integral kernels. This approach was then refined in Grombein et al. (2013) by representing the integral kernels in terms of Cartesian coordinates. Uieda et al. (2015) numerically evaluated the gravitational effect of a tesseroid using Gauss-Legendre quadrature formulas and Marotta and Barzaghi (2017) proposed the computation of the potential and gravitational effects of a tesseroid in a rotated frame, wherein these quantities were evaluated by means of the effect of a sector of a spherical zonal band. Recently, Lin and Denker (2019) developed a method for computing the gravitational effects of a tesseroid, which combined the Gauss-Legendre quadrature and Taylor series expansion of the integral kernel up to the second order. In this paper, the methods proposed in Heck and Seitz (2007) and Marotta and Barzaghi (2017) were compared. The approach involved either comparing the two methods by employing closed formulas defining the potential and gravity of known spherical mass distributions (e.g., the spherical shell) or by performing direct comparison of the tesseroid effect computed using the two methods. Section 2 presents an overview of the two approaches. In Section 3, the closed formula effects pertaining to the gravity and potential of a spherical shell and zonal bands are compared with the corresponding values computed using the two approaches. Furthermore, a direct comparison between the effects of a given tesseroid, as computed by the two methodologies, is performed. Finally, the results are discussed in Section 4.

2. FORWARD MODELLING

Forward modelling in the space domain is a very important task in geodesy and other geo-sciences. It is based on the representation of the gravitational potential V by the Newton integral:

$$V = G \iiint_{\Omega} \frac{\rho}{\ell} d\Omega , \quad (1)$$

where G is the Newton's gravitational constant, ρ is density (a point function), ℓ is the Euclidean distance between the (attracted) observation point P and the running integration

point (source- or mass-point) Q , and $\Omega \subset \mathbb{R}^3$ is the integration domain. The product $\rho d\Omega$ represents differential mass element dm . The gravitational potential G depends on the Euclidean distance ℓ . If a Cartesian coordinate system (x_1, x_2, x_3) is used, ℓ is given as

$$\ell(P, Q) = \sqrt{\Delta x_1^2 + \Delta x_2^2 + \Delta x_3^2} = \sqrt{\Delta x_i \Delta x_i}. \quad (2)$$

In terms of geocentric spherical coordinates r, φ, λ (radius from the Earth's center, geocentric latitude and longitude, respectively), the distance between $P(r, \varphi, \lambda) \in \mathbb{R}^3$ and $Q(r', \varphi', \lambda') \in \Omega$ can be defined using the variables shown in Fig. 1 as

$$\ell(P, Q) = \sqrt{r^2 + r'^2 - 2rr' \cos \psi}, \quad (3)$$

where ψ is the spherical distance between the geocentric position vectors of P and Q and is defined as

$$\cos \psi(P, Q) = \sin \varphi \sin \varphi' + \cos \varphi \cos \varphi' \cos(\lambda - \lambda'). \quad (4)$$

Several approaches can be used to discretize the masses which have to be considered to compute the effect on the gravitational potential or functionals of the potential. The approaches depend on the coordinate system used (Cartesian, geographical, geocentric spherical, etc.) and the kind of finite shape of discretisation of the masses. The commonly used geometrical mass decompositions are summarized in the following subsections.

2.1. Idealized mass discretizations

Several possibilities exist to arrange the masses in a very idealized manner. The main considerations to select an approach include simplifying the analytical problem that is under consideration or considerably reducing the numerical effort. The latter may suffer from a loss of accuracy if the distance ℓ is small (near zone); in contrast, significant simplification may be realized if the distance ℓ is large (far zone) with a sufficiently small approximation error.

2.1.1. Point mass

From Eq. (1) the potential of a point mass m can be defined as follows:

$$\delta V = G \frac{m}{\ell}. \quad (5)$$

From the potential theory (cf. *Torge and Müller, 2012*), it is well known that the isotropic potential holds for a point mass, a homogeneous sphere ($\rho = \text{constant}$), as well for a sphere with a radial varying density function $\rho(r)$.

2.1.2. Mass line

The mass distribution of a vertical cylinder or prism can be approximated by a vertical mass line s . The potential of a mass line can be defined as follows:

$$\delta V = G \int_s \frac{\rho}{\ell} ds. \quad (6)$$

2.1.3. Surface layer

From an analytical point of view, the potential of a single surface layer with surface density μ is of interest. It is defined using the surface integral:

$$\delta V = G \iint_A \frac{\mu}{\ell} dA. \quad (7)$$

This potential, for example, it is used when solving the scalar Molodenskii problem (*Moritz, 1980*).

2.2. Volumetric mass discretization

In real applications, we deal with volumetric mass distributions, which are obtained using digital terrain models (DTM). In particular, the masses in the vicinity of the observation point exert a dominant influence on the potential or its functionals; therefore, their geometric approximation must be optimized to ensure that the approximation error and the computing costs are as small as possible. The ideal geometry depends on the coordinate system in which the DTM is represented.

2.2.1. Rectangular prism

If the modelling is performed in Cartesian coordinates, the axes of the system are orthogonal to each other. The integral (1) has a closed analytical solution if the edges of the prism are parallel to the base vectors of the so-called prism system. The somewhat elongated formulas were derived by *Mader (1951)* and given by *Heck and Seitz (2007)*. These formulas were optimized by *Grüninger (1990)* and discussed by *Nagy (1966)* and *Nagy et al. (2000, 2002)* in the context of numerical problems that occur if the observation point lies in one of the delimiting planes of the prism. The advantage of the prism formulas, which pertains to its closed analytical representations of potential and derivatives, is mitigated by at least four limitations. (1) The formulas cannot strictly represent a spherical mass distribution, and they have a horizontal, planar top-surface; (2) the observation point P must be transformed into the system of the prism; (3) in case of gravitational attraction and gravity gradients, the vector/matrix must finally be rotated into the system of the observation point; and (4) the CPU-costs are extremely high compared to alternative discretization due to the several log and arctan functions involved.

2.2.2. Polyhedron

A polyhedron is a body with a more general geometry as the special case of a prism. Several authors have elaborated expressions for the gravitational potential and derivatives

of polyhedral-shaped bodies (cf. Hamayun *et al.*, 2009; Tsoulis *et al.*, 2009; D'Urso, 2013, 2014; Ren *et al.*, 2017, 2018; Chen *et al.*, 2018; Zhang and Chen, 2018).

2.2.3. Potential and gravity of a tesseroid

Global as well as regional and local mass models are parametrized in spherical coordinates. These polar coordinates generate the horizontal bounds of a tesseroid. The East-West limitation is established using a pair of meridional planes with λ_1 and $\lambda_2 = \text{constant}$. Two (concentric) coaxial circular cones define the bounds in the North-South direction. The respective cone angles are given by the parallels φ_1 and $\varphi_2 = \text{constant}$. The top and bottom are generated by concentric spheres of radii r_1 and $r_2 = \text{constant}$. Fig. 1 shows the geometry and associated parameters of a spherical tesseroid.

Although the tesseroid is defined by geocentrically spherical coordinates, the potential generated by the tesseroid can be described in other coordinates. The most obvious, albeit natural, are spherical coordinates, which are also used in the present study. A presentation based on Cartesian coordinates has been reported by Grombein *et al.* (2013), for the potential, gravity vector and the gravitational tensor elements.

2.2.4. GIK approach

The potential, gravitational effect and gravity gradients of a spherical tesseroid with the geometry shown in Fig. 1 can be computed according to the approach presented in Heck and Seitz (2007), Wild-Pfeiffer (2008) and Grombein *et al.* (2013). In the following section, the basic concepts for deriving the analytical presentation of the tesseroid formulas according to the GIK approach are outlined for the potential. Starting from the Newton's integral given in Eq. (1), the gravitational potential δV of a single tesseroid with a constant mass density ρ and with integration limits written in spherical coordinates

$$\delta V(r, \varphi, \lambda) = G\rho \int_{\lambda_1}^{\lambda_2} \int_{\varphi_1}^{\varphi_2} \int_{r_1}^{r_2} \frac{r'^2 \cos \varphi'}{\ell(P, Q)} dr' d\varphi' d\lambda' \quad (8)$$

is of the elliptical integral type. Therefore, no closed analytical solution exists for Eq. (8). The angle between the position vectors of the observation point $P(r, \varphi, \lambda)$ and the integration point $Q(r', \varphi', \lambda')$ is denoted by ψ and has been already defined in Eq. (4). To obtain an approximative analytical solution, the integral kernel in Eq. (8)

$$K(P, Q) = \frac{r'^2 \cos \varphi'}{\ell(P, Q)} \quad (9)$$

is expanded into a Taylor series

$$K(P, Q) = \sum_{i,j,k} \frac{K_{ijk}}{i!j!k!} (r' - r_0)^i (\varphi' - \varphi_0)^j (\lambda' - \lambda_0)^k. \quad (10)$$

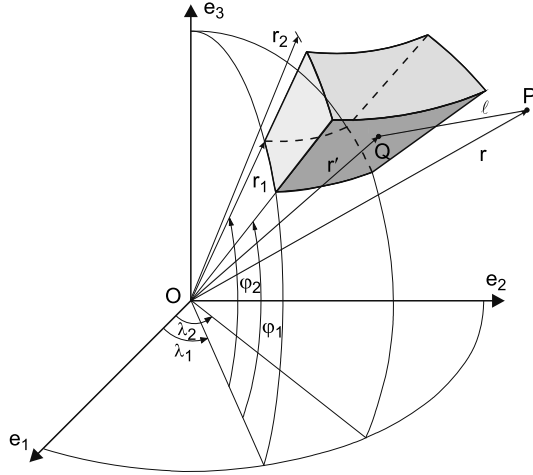


Fig. 1. Geometry of a spherical tesseroid, modified from *Heck and Seitz (2007)*.

The Taylor point $Q_0(r_0, \varphi_0, \lambda_0)$ is placed at the geometrical centre of the tesseroid. The partial derivatives of the kernel function K are given in *Heck and Seitz (2007)*. The zero-order coefficient K_{000} is evaluated at the Taylor point Q_0 :

$$K_{000} = \frac{r_0^2 \cos \varphi_0}{\ell_0}, \quad \text{with } \ell_0 = \sqrt{r^2 + r_0^2 - 2rr_0 \cos \psi_0}, \quad (11)$$

and

$$\cos \psi_0 = \sin \varphi \sin \varphi_0 + \cos \varphi \cos \varphi_0 \cos(\lambda - \lambda_0). \quad (12)$$

The second-order coefficients K_{200} , K_{020} and K_{002} can be consulted in *Heck and Seitz (2007)*. The terms of the fourth and higher order are neglected in this paper. Fourth order terms have been elaborated by *Shen and Deng (2016)*, but they are listed in a non-simplified manner. Inserting the Taylor series (10) into (8), replacing the kernel K , and performing the integration with respect to the Taylor steps, yields the power series

$$\delta V(r, \varphi, \lambda) = G\rho \Delta r \Delta \varphi \Delta \lambda \times \left[K_{000} + \frac{1}{24} \left(K_{200} \Delta r^2 + K_{020} \Delta \varphi^2 + K_{002} \Delta \lambda^2 \right) + \mathcal{O}(\Delta^4) \right], \quad (13)$$

where the Landau symbol $\mathcal{O}(\Delta^4)$ indicates that the omitted Taylor terms are of the fourth and higher order. Terms of even degree vanish due to the existence of symmetry with respect to the Taylor point.

Considering the series of terms of zero-order in Eq. (13) and representing K_{000} by its expression from Eq. (11), the mass term of zero-order approximation can be defined as:

$$m_0 = \rho \Delta r \Delta \varphi \Delta \lambda K_{000} \ell_0 = \rho \Delta r \Delta \varphi \Delta \lambda r_0^2 \cos \varphi_0 = \rho (\Delta r) (r_0 \Delta \varphi) (r_0 \cos \varphi_0 \Delta \lambda). \quad (14)$$

The gravitational effect of a tesseroid can be defined using the partial derivative of the potential δV with respect to the geocentric distance r

$$\delta g(r, \varphi, \lambda) = -\frac{\partial \delta V(r, \varphi, \lambda)}{\partial r} = G \rho \int_{\lambda_1}^{\lambda_2} \int_{\varphi_1}^{\varphi_2} \int_{r_1}^{r_2} L(P, Q) dr' d\varphi' d\lambda'. \quad (15)$$

The same procedure as that described for the potential can be applied to the kernel L :

$$L(P, Q) = \frac{r'^2 (r - r' \cos \psi) \cos \varphi'}{\ell^3(P, Q)}. \quad (16)$$

The corresponding tesseroid formulas were first published by *Wild-Pfeiffer (2008)*. Optimized formulas were applied to GOCE gradients by *Grombein et al. (2014)* to smooth the measured second derivatives. Further refinements of this method were performed in *Grombein et al. (2013)*, wherein the optimized formulas were derived based on Cartesian integral kernels. The tesseroid formulas based on Cartesian coordinates are even more effective than those in spherical coordinates in terms of the required computational time. It should be noted that integration with respect to r is possible in the closed analytical form (cf. *Martinec, 1998; Heck and Seitz, 2007*). Based on this fact, *Lin and Denker (2019)* derived expressions for the gravitational effect of a tesseroid with linearly varying density.

2.2.5. UNIPOL approach

The UNIPOL approach starts from the well-known result that a general closed formula of the volume integral (1) does not exist; however, it exists when the observation point is located along the polar axis (see, e.g., Le Fehr, 1991) and a tesseroid coincides with the sector of a spherical zonal band of a spherical cap. In this case the closed analytical solution for the gravitational contribution of the tesseroid is

$$\delta g = \frac{G \rho}{r^2} \Delta \lambda (I_1 + I_2 + I_3 + I_4 + I_5), \quad (17)$$

with

$$I_1 = \frac{1}{3} \left[(R+h)^2 + r^2 (3 \cos^2 \varphi_2 - 2) + r(R+h) \cos \varphi_2 \right] \times \sqrt{(R+h)^2 + r^2 - 2r(R+h) \cos \varphi_2}, \quad (18)$$

$$I_2 = -\frac{1}{3} \left[R^2 + r^2 \left(3 \cos^2 \varphi_2 - 2 \right) + rR \cos \varphi_2 \right] \sqrt{R^2 + r^2 - 2r(R+h) \cos \varphi_2}, \quad (19)$$

$$I_3 = -\frac{1}{3} \left[(R+h)^2 + r^2 \left(3 \cos^2 \varphi_1 - 2 \right) + r(R+h) \cos \varphi_1 \right] \times \sqrt{(R+h)^2 + r^2 - 2r(R+h) \cos \varphi_1}, \quad (20)$$

$$I_4 = \frac{1}{3} \left[R^2 + r^2 \left(3 \cos^2 \varphi_1 - 2 \right) + rR \cos \varphi_1 \right] \sqrt{R^2 + r^2 - 2r(R+h) \cos \varphi_1}, \quad (21)$$

$$I_5 = -\cos \varphi_2 \sin^2 \varphi_2 r^3 \times \ln \left(\frac{\sqrt{(R+h)^2 + r^2 - 2r(R+h) \cos \varphi_2} + (R+h) - r \cos \varphi_2}{\sqrt{R^2 + r^2 - 2r(R+h) \cos \varphi_2} + R - r \cos \varphi_2} \right). \quad (22)$$

The UNIPOL approach is thus based on the rotation of each tesseroid from the global Earth-Centred Rotational (ECR) reference frame into the local Earth-Centred *P*-Rotational (ECP) reference frame, having the same origin *O* and polar axis coinciding with the line connecting *O* to the observation point *P* (Fig. 1), aiming at making the rotated tesseroids suitable to be handled as a sector of a spherical zonal band of a spherical cap, thus making possible the application of the corresponding analytical solution. Two procedures, namely, the RT and ST procedures, are developed for the practical implementation of the mapping operation according to the spherical distance of the tesseroid from the observation point.

The RT procedure is based on a forced re-orientation of the rotated spherical tesseroids (pink areas in Fig. 2b) around their centre to form sectors of a spherical band (red lines in Fig. 2b) that develop along the meridian of the local ECP meridians and have dimensions along the ECP-longitude and the ECP-latitude such that each sector maintains the same area of the original tesseroid. The results of the sensitivity tests performed to verify the effects of the re-orientation on the gravitational contribution of a tesseroid show that, for a DTM resolution of 1', the maximum difference is of the order of 10–20 mGal; this difference rapidly decreases with distance and becomes less than 1 µGal at an angular distance of approximately 0.1°. The ST procedure involves a local second-order decomposition of each tesseroid into a number N_s of small equal-area sectors of a spherical band, which develop along the local ECP meridians and parallels (blue lines in Fig. 2c). The sensitivity tests demonstrate that the ST procedure converges to a stable value for a suitable N_s , which varies with latitude, decreasing from the equator to the North Pole. In the present study, we make N_s vary linearly from the equator to the North Pole, from 200 to 20. Comparative tests show that for $N_s = 1$, the ST procedure is equivalent to the RT procedure, and the gravitational contribution is underestimated. Furthermore, for a tesseroid with the dimensions $\Delta\varphi \times \Delta\lambda = 1' \times 1'$ the RT procedure is adequate at distances $\geq 0.1^\circ$ from the observation point; a more accurate ST procedure is required at distances closer to the observation point *P*.

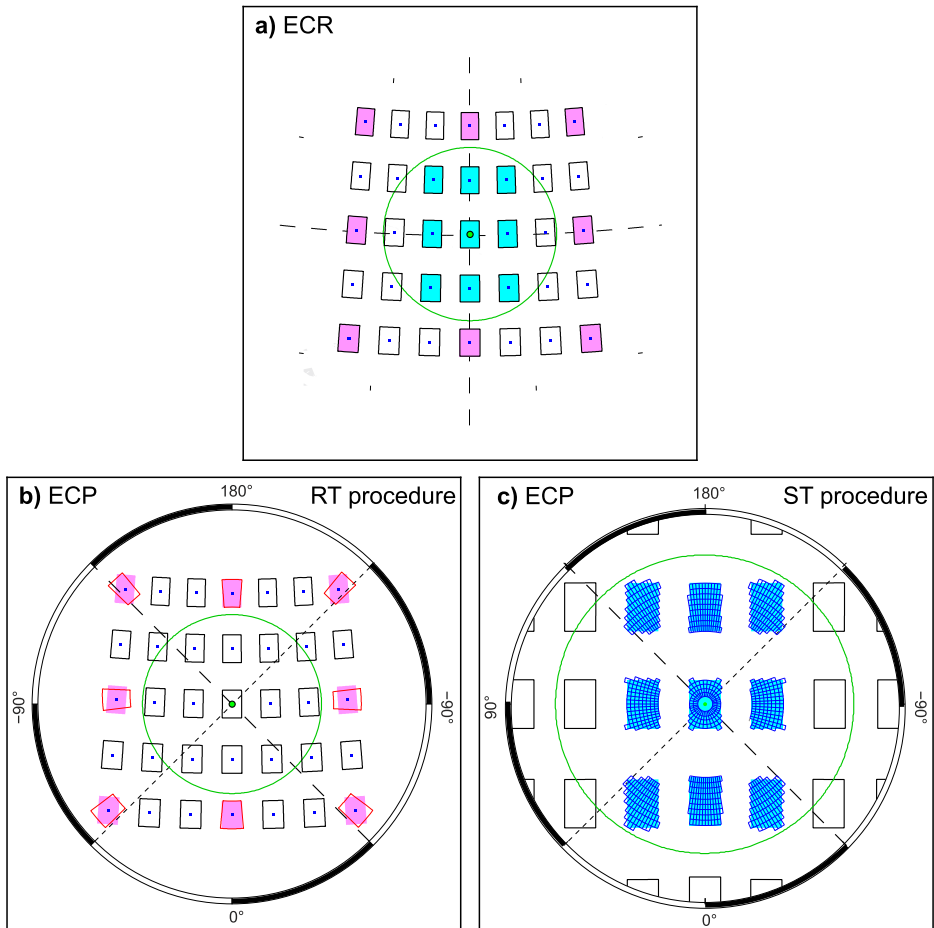


Fig. 2. General scheme of the UNIPOL approach. **a)** Example of a set of tesseroids in the Earth-Centred Rotational (ECR) reference frame. **b)** RT procedure: rotated tesseroids (pink areas) and corresponding re-oriented tesseroids (red sectors) in the local Earth-Centred P -Rotational (ECP) reference frame. **c)** ST procedure: rotated tesseroids (cyan areas) and corresponding decomposition into sectors of a spherical band (blue sectors) in the local ECP reference frame. The green circlet in the center of the sketch indicates the observation point. The green solid circle around point P , where the tesseroids reside at a distance $\leq 0.1^\circ$ from the observation point and the ST procedure is required. Modified from Marotta and Barzaghi (2017).

2.3. Solving Newton's integral by numerical integration

Instead of resolving Newton's integral in a closed analytical or approximate manner, purely numerical methods can also be applied. In geodesy, the solution of two-dimensional integrals is an application of the Gauss-Legendre squaring. For three-dimensional problems, the Gauss-Legendre cubature formulas are used (Uieda *et al.*,

2015). A numerical comparison of analytical and numerical methods and their adaption for solving for the potential, gravity and gravitational tensor elements can be found in Wild-Pfeiffer (2008).

2.3.1. Mass of a tesseroid and a prism

To compare the prism and the tesseroid approach in terms of their approximation quality, as described in Section 3, the two bodies should have the same mass. The dimensions of the prism are computed from the specified dimensions of the tesseroid as follows. The mass of a spherical tesseroid with constant mass density ρ can be solved in closed analytical form, as reported by Grüninger (1990):

$$m^T = \rho \int_{\lambda_1}^{\lambda_2} \int_{\varphi_1}^{\varphi_2} \int_{r_1}^{r_2} r'^2 \cos \varphi' dr' d\varphi' d\lambda' = \frac{1}{3} \rho (r_2^3 - r_1^3) (\sin \varphi_2 - \sin \varphi_1) (\lambda_2 - \lambda_1). \quad (23)$$

Performing the series expansion of m^T at the Taylor point $Q_0(r_0, \varphi_0, \lambda_0)$

$$\begin{aligned} m^T &= \rho r_0^2 \cos \varphi_0 \Delta r \Delta \varphi \Delta \lambda \left[1 + \frac{1}{12} \left(\frac{\Delta r}{r_0} \right)^2 - \frac{1}{24} (\Delta \varphi)^2 + \mathcal{O}(\Delta^3) \right] \\ &= m_0 \left[1 + \frac{1}{12} \left(\frac{\Delta r}{r_0} \right)^2 - \frac{1}{24} (\Delta \varphi)^2 + \mathcal{O}(\Delta^3) \right], \end{aligned} \quad (24)$$

and comparing the expression with the tesseroid formula for the potential $\delta V(P)$ discloses that the zero-order approximation of $\delta V(r, \varphi, \lambda)$ in Eq. (13) is nothing more than the isotropic potential of a point mass m_0 :

$$\begin{aligned} \delta V_0(r, \varphi, \lambda) &= G \rho \Delta r \Delta \varphi \Delta \lambda K_{000} \left(1 + \mathcal{O}(\Delta^2) \right) \\ &= G \rho \Delta r \Delta \varphi \Delta \lambda \frac{r_0^2 \cos \varphi_0}{\ell_0} \left(1 + \mathcal{O}(\Delta^2) \right) = \frac{G m_0}{\ell_0} \left(1 + \mathcal{O}(\Delta^2) \right). \end{aligned} \quad (25)$$

The mass of a prism is simply given by

$$m^P = \rho \Delta x \Delta y \Delta z, \quad (26)$$

where the dimensions of the prism are denoted by Δx , Δy and Δz . They refer to the orthogonal coordinate system of the prism. From the required condition of mass equality, the dimensions of the equivalent prism, specifically Δr , $\Delta \varphi$ and $\Delta \lambda$, can be obtained by Eqs (24) and (26) as follows:

$$\begin{aligned} m^T &= \rho r_0^2 \cos \varphi_0 \Delta r \Delta \varphi \Delta \lambda \left[1 + \frac{1}{12} \left(\frac{\Delta r}{r_0} \right)^2 - \frac{1}{24} (\Delta \varphi)^2 + \mathcal{O}(\Delta^3) \right] \\ &= m^P = \rho \Delta x \Delta y \Delta z. \end{aligned} \quad (27)$$

Identifying the height of the prism Δr with the height of the spherical tesseroid

$$\Delta z = \Delta r, \quad (28)$$

and neglecting the terms of order $\mathcal{O}(\Delta^2)$, the horizontal coordinates of the prism are

$$\Delta x = r_0 \Delta\varphi, \quad \Delta y = r_0 \cos\varphi \Delta\lambda. \quad (29)$$

The maximum relative error in the volume, caused by neglecting the $\mathcal{O}(\Delta^2)$ terms, reaches 10^{-5} for $|\Delta\varphi|=1^\circ$ and $|\Delta r| \leq 9000$ m.

3. NUMERICAL INVESTIGATIONS BASED ON THE GIK AND UNIPOL APPROACH

To compare the numerical results obtained using the two approaches based on tesseroid discretization we compute the potential and gravity due to three different mass distributions: (1) a spherical shell, (2) zonal bands and (3) one $1^\circ \times 1^\circ$ tesseroid centred at ($\varphi=45^\circ$, $\lambda=45^\circ$). The first two scenarios provide an analytical solution and the comparison is performed in terms of the approximation errors. For the third scenario, we focus on the numerical difference between the approaches and the computational time.

For all subsequent numerical comparisons, the mass density is set to a constant value $\rho=2670$ kg m⁻³. The value of $G=0.66720 \times 10^{-10}$ m³ kg⁻¹ s⁻² is adopted for the Newton's gravitational constant.

3.1. Test scenario 1: Spherical shell

The closed analytical solution for the isotropic potential of a spherical shell of constant mass density ρ at the observation point P can be specified as

$$V^{shell}(r_P) = \frac{4}{3}\pi G\rho(r_2^3 - r_1^3)\frac{1}{r_P}, \quad r_P \geq r_2 \geq r_1. \quad (30)$$

Its negative radial partial derivative (gravitational attraction) is

$$g^{shell}(r_P) = \frac{4}{3}\pi G\rho(r_2^3 - r_1^3)\frac{1}{r_P^2}, \quad r_P \geq r_2 \geq r_1, \quad (31)$$

(cf. Heck and Seitz, 2007; Vaníček et al., 2001, 2004), where r_1 and r_2 denote the internal and external radius of the spherical shell, respectively, and r_P is the geocentric distance of the observation point P .

The constant radius of the sphere on which the shell is set up is $R=r_1=6378137$ m throughout the computations.

To validate the tesseroid methods, the thickness of the spherical shell is set to $d \in \{1000 \text{ m}, 2000 \text{ m}\}$ and the geocentric distance of the observation point varies with $H_P = r_P - r_2 \in \{1000 \text{ m}, 2000 \text{ m}, 3000 \text{ m}, 4000 \text{ m}, 10000 \text{ m}\}$.

The analytical (exact) values of the potential and gravity are specified in Table 1 and 2, respectively. The analytical values of both potential and gravity change very gradually with the height H_P , while the values approximately double for a double value of shell thickness.

Due to the rotational symmetry of the shell, when the two approaches are used, the computation of the potential and gravity can be restricted to a grid located along the (arbitrary) meridian ($\lambda = 0^\circ$). The grid spacing is set to $\Delta\varphi = 10'$.

In previous studies, the GIK tesseroid approach was first applied to determine the effect of potential and gravitational attraction, and it was compared analytically and numerically with the prism method and point mass discretization. In particular, *Heck and Seitz (2007)* presented the outstanding advantage of the tesseroid method in reducing the computational time by 90% compared to the numerical evaluation of prisms. Further refinements of the method in terms of the analytical representation of the potential, gravity and gravitational gradients (δM_{ij}) in Cartesian coordinates were made by *Grombein et al. (2013)*. In addition to the fact that they lead to further reduction in the computational costs (see Table 4 later), the tesseroid formulas for the gravitational gradients in Cartesian coordinates have no singularity at the poles.

Previous findings by the UNIPOL approach (*Marotta and Barzaghi, 2017*), based on the analysis of the sole gravity contribution, can be summarized as follows: a) regardless of the number of sectors in which the shell is decomposed, the difference between the analytical and computed solution for a spherical shell is not affected by the height of the

Table 1. Values obtained using analytical formula for the potential of a spherical shell (V^{shell}). H_P : height of the observation point, d : thickness of the shell.

H_P [m]	d [m]	
	1000	2000
	V^{shell} [$m^2 s^{-2}$]	
1000	14278.1194217969	
2000	14275.8815200995	28556.2395452924
3000	14273.6443198137	28551.7644431993
4000	14271.4078206098	28547.2907434897
10000		28520.4779584068

Table 2. The same as in Table 1, but for the gravitational attraction (g^{shell}).

H_P [m]	d [m]	
	1000	2000
	g^{shell} [$m s^{-2}$]	
1000	-223.8252513122	
2000	-223.7550936618	-447.5803504735
3000	-223.6849689924	-447.4400791458
4000	-223.6148772834	-447.2998737490
10000		-446.4600236095

observation point; b) the absolute error increases with increasing column size; c) the error is of the order of a few μGal . Figures 3 and 4 show the new findings of the present comparative analysis performed using the GIK and the UNIPOL approaches.

Figure 3 shows that the approximation errors for both approaches (represented by solid and dotted curves for GIK and UNIPOL, respectively) are more or less constant with varying latitude. Particularly, for the GIK approach, if the observation point P reaches the Pole, the error increases, while it strongly decreases with increasing height H_P . In contrast, for the UNIPOL approach, the error is not affected by H_P , and it decreases when the observation point approaches the North Pole. Furthermore, while the UNIPOL approach reproduces the analytical values of the potential better than the GIK approach when the observation point resides at the top of the shell (blue dots in panel a and green dots in panel b), the GIK approach performs better at greater heights H_P (cyan, red and

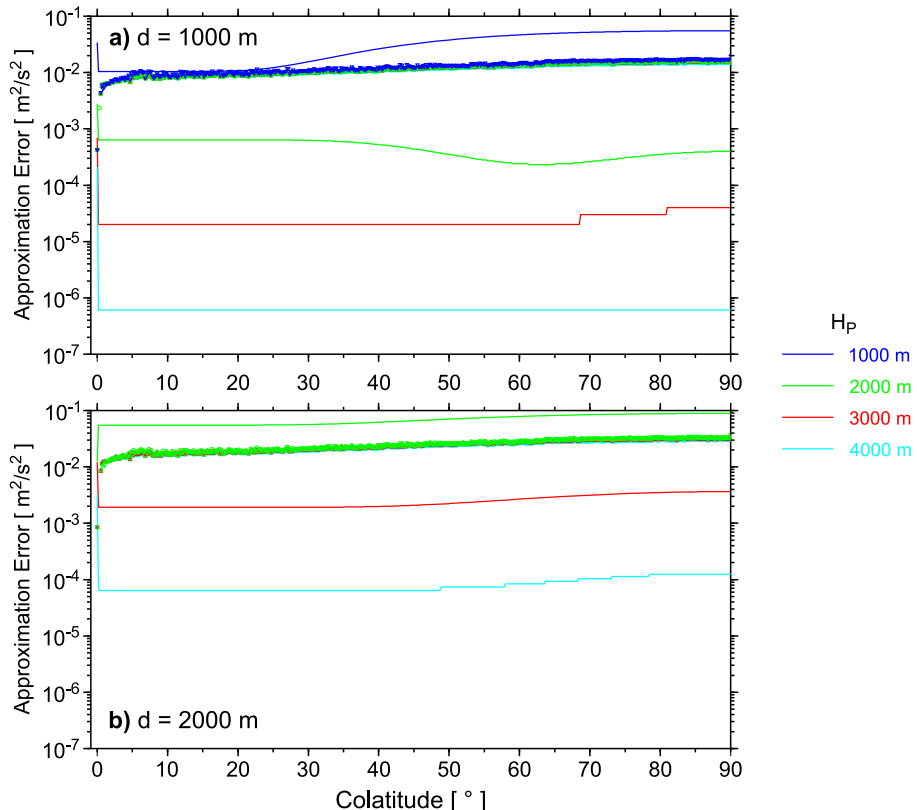


Fig. 3. Approximation error of the potential along a meridian for GIK (solid curves) and UNIPOL (dots, overlapping) approaches, for a thickness d of the spherical shell of **a)** 1000 m and **b)** 2000 m for different heights H_P of the observation point. Note that the approximation errors for the UNIPOL method at different heights are very similar at the range of 1 to $3 \times 10^{-2} \text{ m}^2 \text{ s}^{-2}$.

green curves in panel a, cyan and red curves in panel b). Nevertheless, the relative error is less than 10^{-6} for both approaches.

Figure 4 shows that the approximation error of gravity is more or less constant with latitude in the case of the GIK approach (solid curves). In contrast, when the UNIPOL approach is used the approximation error spreads within a dispersion band that widens at the higher latitudes. In the meantime, the approximation error decreases towards the North Pole. The UNIPOL approach reproduces the analytical solution better than the GIK approach does when the observation point resides at the top of the shell (blue dots in panel a and green dots in panel b) and for $H_P = 3000$ m and $d = 2000$ m (red dots in panel b). However, when the vertical distance between the observation point and the surface of the shell is greater than 2000 m the GIK approach performs better. The worst relative error is of the order of 10^{-2} and 10^{-1} , for the UNIPOL and GIK approaches, respectively. The dispersion characterizing the approximation error of gravity computed by the UNIPOL approach is ascribable to the specific local tesseral discretization of the UNIPOL approach, which is particularly sensitive to the inverse of the square distance.

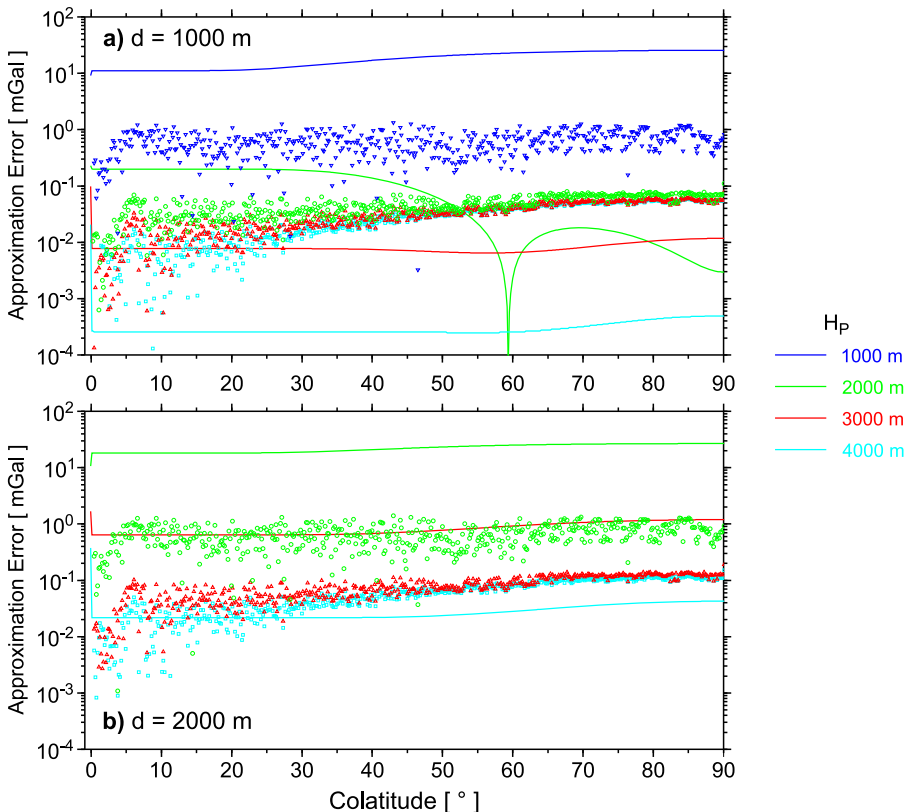


Fig. 4. The same as in Fig. 3, but for the gravitational attraction.

Additionally, gravity is more susceptible than potential against the approximation by tesseroids. Consequently, the discretization of DTM must be performed at a higher resolution or the mass elements of the immediate neighbourhood must be evaluated using prisms. The latter approach is shown in Figs 5 and 6 for the GIK approach.

3.2. Test scenario 2: Zonal bands

In this test, the spherical shell is subdivided into zonal bands, as illustrated in Fig. 7. While the extension of a tesseroid in the North-South direction is $\Delta\varphi = \varphi_2 - \varphi_1$ (cf. Fig. 1), the width of a zonal band is $\Delta\psi = \psi_2 - \psi_1$. In this numerical study, the width of

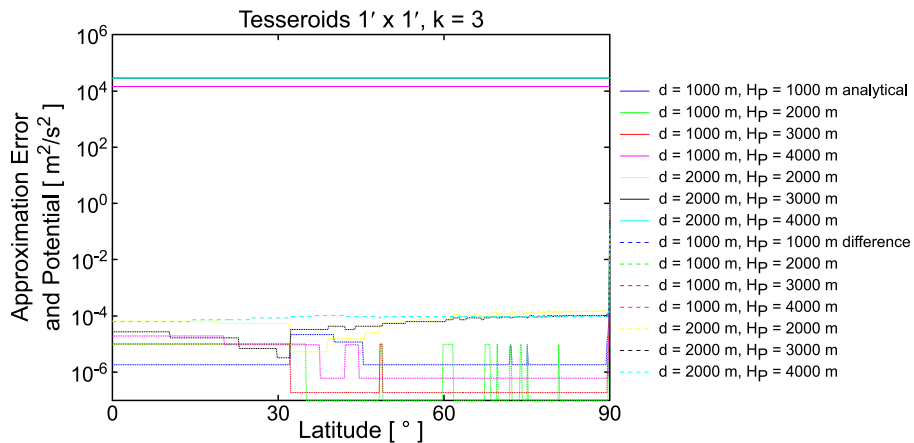


Fig. 5. Approximation error and potential along a meridian when using 3×3 prisms in the neighbourhood.

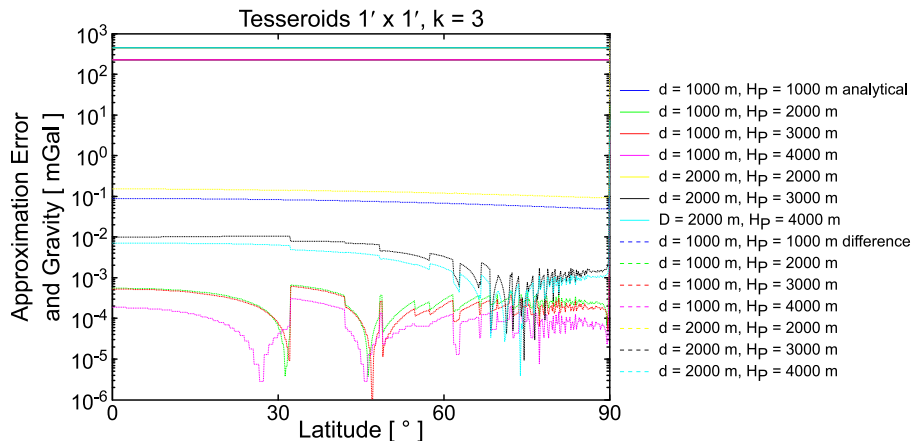


Fig. 6. The same as in Fig. 5, but for the gravitational attraction.

a zonal band is set to $\Delta\psi = 60'$. For the GIK approach the observation point P is located at the North Pole, with the height $H_P = r_P - r_2 \in \{1000 \text{ m}, 2000 \text{ m}\}$.

If the observation point P is located at the Pole also for the UNIPOL approach, neither the RT nor the ST procedure is applied, since the tesseroids are already spherical sectors of a spherical zonal band, and the corresponding solution is a simple numerical summation of the corresponding analytical solutions. To make the comparison with the analytical solution meaningful, when the UNIPOL method is used, the observation point is located at the equator, on one arbitrary meridian ($\lambda = 0^\circ$) and the spherical bands are built with spherical tesseroids of dimension $\Delta\varphi \times \Delta\lambda = 1' \times 1'$ located at a spherical distance $\varphi_2 \leq \varphi \leq \varphi_1$ from the observation point.

As can be seen in Fig. 8 the analytical contribution (black solid curves) of a zonal band to the potential remains over a large spherical range in the same order of magnitude. This is obvious from the fact that the Euclidean distance increases with increase in the masses of the zonal band until the zonal band reaches the Equatorial region as a function of the Euclidean distance.

When the potential is computed by the GIK method, the approximation error within the zonal band nearest to the observation point (polar cap) is large if P is located on the shell and it decreases with increasing height H_P (coloured triangles). For all the other zonal bands, the approximation error decreases rapidly to 10^{-9} to $10^{-8} \text{ m}^2 \text{ s}^{-2}$, which is equivalent to a relative error of less than 10^{-8} . The approximation error increases with increasing spherical distance, with a maximum change greater than one order of magnitude.

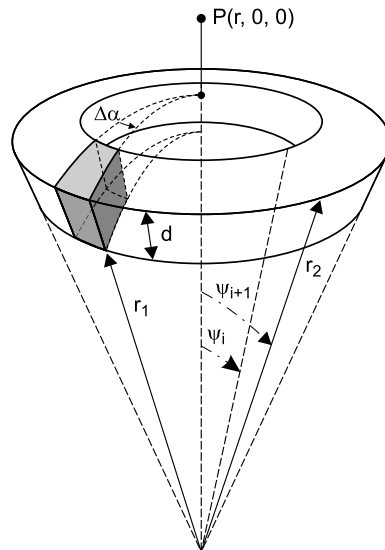


Fig. 7. Geometry of a spherical zonal band and a tesseroid.

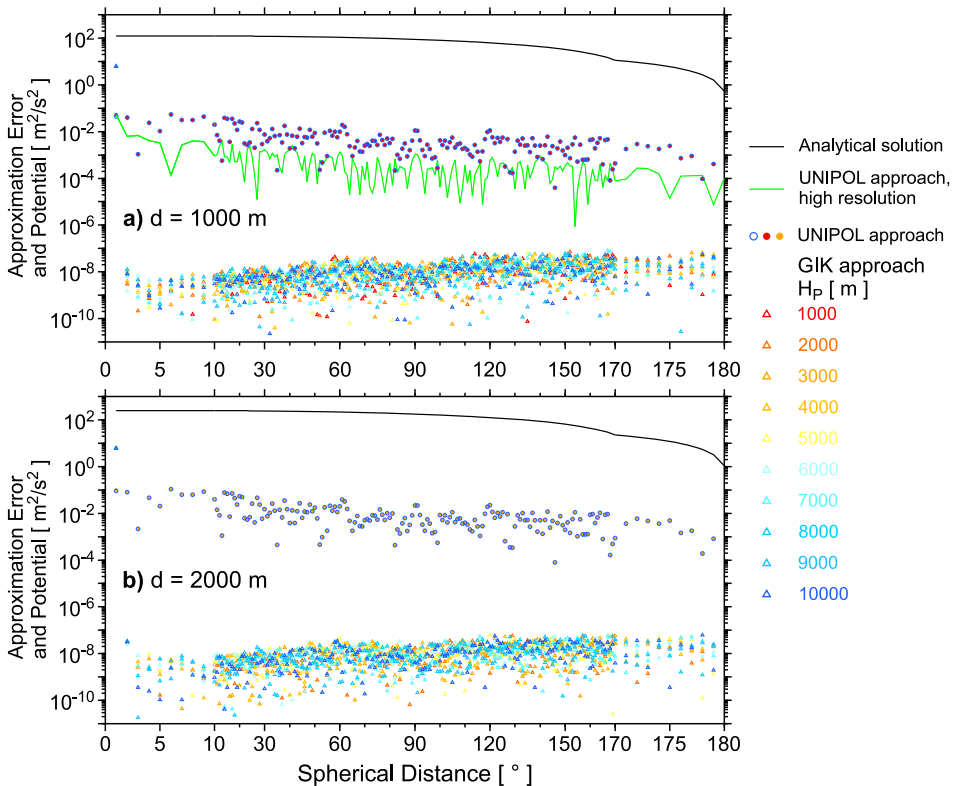


Fig. 8. Approximation error for the potential of a spherical zonal band, determined using the GIK and UNIPOL approaches, with thickness d of a) 1000 m and b) 2000 m. The extension of the band is $\Delta\psi = 1^\circ$ and the horizontal size of the used tesseroids are $\Delta\varphi \times \Delta\lambda = 1' \times 1'$. The green curve in a) shows the approximation error for UNIPOL for a high resolution of $\Delta\varphi \times \Delta\lambda = 0.2' \times 0.2'$.

When the potential is computed by the UNIPOL method, the approximation error is in the mean $10^{-3} \text{ m}^2 \text{ s}^{-2}$, (coloured circles), and it decreases with increasing spherical distance. Although there is a relatively larger approximation error on the potential obtained by the UNIPOL approach, it remains well below the present-day precision of observations (corresponding to an effect on the geoid undulation smaller than 0.1 mm) and it is independent from the height H_P of the observation point.

For both GIK and UNIPOL approaches, no remarkable differences exist in the behaviour of the approximation error if $H_P = 1000 \text{ m}$ or 2000 m . The only notable difference is the magnitude of the potential of the zonal bands.

A similar behaviour is observed when gravity is considered (Fig. 9). Specifically, for the gravity as well, the analytical contribution of a zonal band remains over a large spherical range in the same order of magnitude.

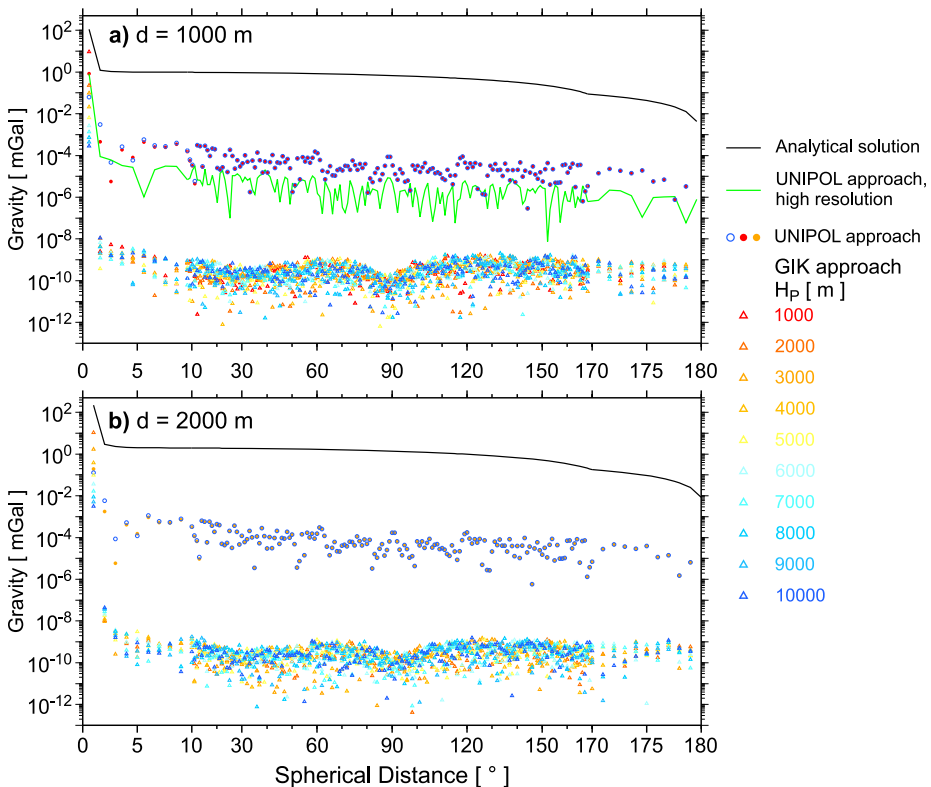


Fig. 9. The same as in Fig. 8, but for gravity.

When the gravity contribution of a zonal band is computed by the GIK method, the approximation error within the first zonal band nearest to the observation point (spherical cap) is large if P is located on the shell, and it decreases with increasing height H_P . For all the other zonal bands the approximation error decreases rapidly, varying between 10^{-11} and 10^{-9} mGal, corresponding to a relative error below 10^{-8} .

When gravity is computed by the UNIPOL method, the approximation error varies between 10^{-6} and 10^{-3} mGal (coloured circles); it decreases with increasing spherical distance, but it is independent of the height of P . Despite the relative larger approximation error obtained by the UNIPOL approach also for gravity, it remains well below the present-day precision of observation (few μ Gal).

No remarkable difference exists in the behaviour of the approximation error for the case in which $H_P = 1000$ m or 2000 m. The only notable difference is in the magnitude of the gravity of the zonal bands.

We attribute the relatively large difference in the quality of the approximation error between UNIPOL and GIK (several orders of magnitude) to the unfavourable setup of the

test scenario 2 for UNIPOL. A higher discretization of the spherical band, such as the use of $\Delta\varphi \times \Delta\lambda = 0.2' \times 0.2'$ tesseroids, produces a more accurate UNIPOL solution with a decrease in the approximation error of more than one order of magnitude (green curves in Figs 8 and 9).

3.3. Test scenario 3: Contribution of a single tesseroid to a global grid

The focus of this test lies in the direct comparison of the GIK and UNIPOL approaches. In this test scenario there is no analytical solution with which to compare our results; thus, we focus the discussion on the numerical difference of our approaches and on the computational time.

Only one tesseroid is considered which is centred at $\varphi = \lambda = 45^\circ$. The dimensions of this tesseroid are as follows: $\Delta\varphi = \Delta\lambda = 1^\circ$ and $d = 1000$ m. The observation points are distributed over the entire sphere in the nodes of a regular grid with a spacing of $\Delta\varphi = \Delta\lambda = 1^\circ$ at a height of $H_P \in \{1000\text{ m}, 2000\text{ m}\}$.

Explicitly, the nodes are located at

$$\begin{aligned}\varphi_i &= 90^\circ - (i-1)\Delta\varphi, \quad i \in \{1, \dots, 181\}, \\ \lambda_j &= (j-1)\Delta\lambda, \quad j \in \{1, \dots, 361\}.\end{aligned}\quad (32)$$

The tesseroid itself is located on a sphere of radius $R = 6378137$ m. The height of the observation point H_P refers to this sphere.

Previous findings obtained using UNIPOL (*Marotta and Barzaghi, 2017*) indicate that the maximum relative error introduced by the RT procedure in the gravity computation occurs at the centre of the tesseroid; it decreases with the distance and reduces to less than 1 μGal at an angular distance of 0.1° at which the more rigorous ST procedure is needed. In the present analysis, before applying UNIPOL approach, the $1^\circ \times 1^\circ$ tesseroid was subdivided into 3600 $1' \times 1'$ tesseroids.

The extreme values (*min, max*) computed by the two approaches are listed in Table 3. The necessary CPU-costs for the evaluation of one tesseroid are listed in Table 4.

Figures 10–13 illustrate the results of the test in terms of the potential (Figs 10a and 12a) and the gravity (Figs 11a and 13a) contributions obtained by the GIK approach and the corresponding differences between the GIK and the UNIPOL computations (Figs 10b–13b). The specific values of the tesseroid height have only a small impact on the numerical results, which confirms the expected isotropic behaviour, both in the potential and in the gravity attraction. The maximum difference between the two solutions occurs when the observation point is located at the centre of the tesseroid and it is of the order of 10^{-2} m s $^{-2}$ and 10^{-1} mGal, for the potential and gravity, respectively, decreasing to below 10^{-5} m s $^{-2}$ and 10^{-5} mGal, respectively, for spherical distances greater than 5° from the center of the tesseroid.

Table 3. Statistical values for one tesseroid with dimensions $\Delta\varphi = 1^\circ$, $\Delta\lambda = 1^\circ$ and $d = 1000$ m.

H_P [m]	Functional	Approach	<i>min</i>	<i>max</i>
1000	Gravitational Attraction [mGal]	GIK	0.000960	110.82167
		UNIPOL	0.000959	110.91724
		UNIPOL – GIK	0.000001	0.09557
	Gravitational Potential [$m^2 s^{-2}$]	GIK	0.122370	57.71032
		UNIPOL	0.122373	57.69800
		UNIPOL – GIK	0.000003	0.01368
2000	Gravitational Attraction [mGal]	GIK	0.000960	108.60610
		UNIPOL	0.000959	108.99745
		UNIPOL – GIK	0.000001	0.39135
	Gravitational Potential [$m^2 s^{-2}$]	GIK	0.122360	56.61318
		UNIPOL	0.122363	56.59690
		UNIPOL – GIK	0.000003	0.01628

Table 4. Relative computing time (CPU-costs, in %). δV : potential of a tesseroid; δg : corresponding gravitational effect; N_s : number of small equal-area sectors; δM_{ij} : tensor of gravitational gradient.

Approach	Operating System	Method	δV	δg	δM_{ij}
GIK	Linux server, quad core, 3.3 GHz, Intel® Xeon® Processor X5680	Sperical	100	150	800
		Cartesian	80	130	640
		Prisms	1200	800	9000
UNIPOL	MacBook Pro dual core, 2.8 GHz, Intel® Core™ i7	RT	1000		
		ST, $N_s = 20$	1000		
		ST, $N_s = 141$	8000		

4. CONCLUSIONS

We compared two different approaches used to compute the gravitational effects of a tesseroid, namely, the GIK approach (*Heck and Seitz, 2007*), which is based on the Taylor expansion of the integral kernel, and the UNIPOL approach (*Marotta and Barzaghi, 2017*), which maps the tesseroid into sectors of spherical zonal bands. Three benchmark tests were performed. In the first test, the numerical solutions were compared to the analytical solution of a spherical shell; in the second test, the numerical solutions were compared to the analytical solution of the zonal bands; in the final test, the two approaches were compared to each other in terms of numerical differences and computational time in the context of the gravity effect of one $1^\circ \times 1^\circ$ tesseroid.

The relative computational times listed in Table 4 are in good agreement with the experiences reported by *Heck and Seitz (2007)*, *Grombein et al. (2013)* and *Marotta and Barzaghi (2017)*. The investigation comparing the GIK and UNIPOL procedures in the context of CPU-costs and approximation accuracy indicates that the suitability of the methods depends on the project environment.

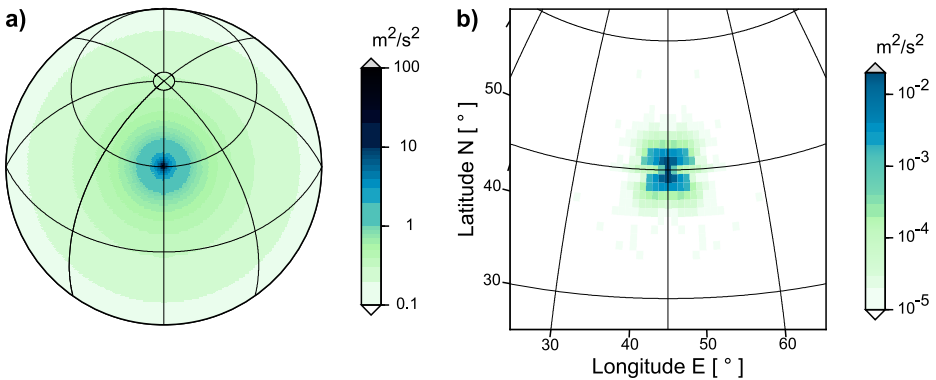


Fig. 10. a) Potential contribution of one tesseroid (45° , 45° , 1 km) obtained by the GIK approach at the height $H_P = 1$ km. b) Corresponding difference between the GIK and UNIPOL computations.

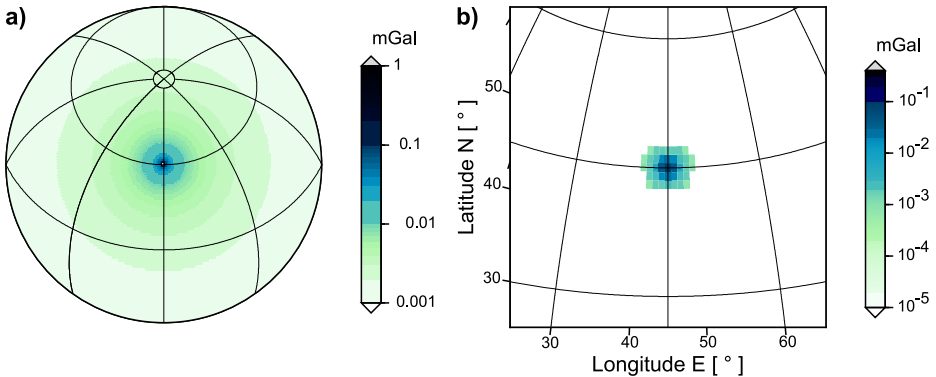


Fig. 11. The same as in Fig. 10, but for the gravity contribution.

In general, both approaches produce a remarkably accurate solution, with a relative error considerably lower than 10^{-6} and 10^{-3} for the potential and gravity, respectively. Nevertheless, the UNIPOL approach reproduces the most accurate solution when the observation point resides at a small vertical distance from the top of the tesseroid, while the GIK performs better at larger vertical distances. The known near-zone problem of the GIK approach can easily be circumvented by working with the prism formula in the immediate near neighbourhood (3×3 elements). The limitation of the UNIPOL is the large CPU-time involved due to the second-order decomposition. However, this aspect can be improved by further optimizing the algorithm using parallel computing techniques.

Acknowledgements: The authors would like to thank associate editor Nico Sneeuw and the two anonymous reviewers for their constructive comments, which helped to improve the quality of this paper. Some of the figures have been made using GMT - The Generic Mapping Tools (Wessel *et al.*, 2013). A.M.Marotta was supported by the ESA funded project "Gravitational Seismology", ITT AO/1-9101/17/I-NB."

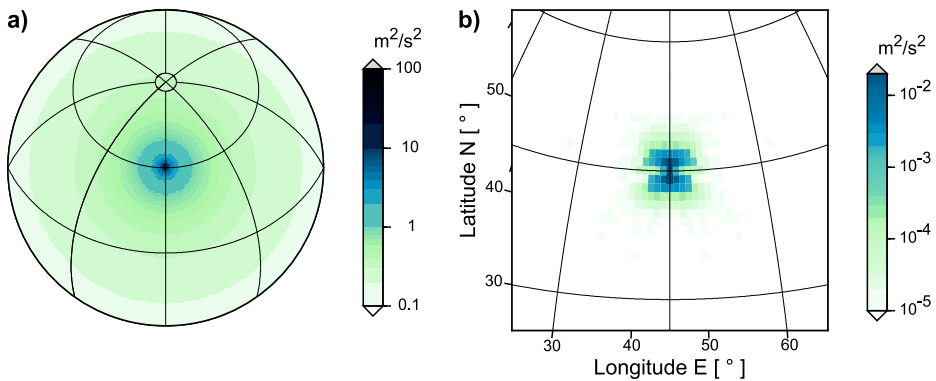


Fig. 12. The same as in Fig. 10, but for the height of $H_P = 2$ km.

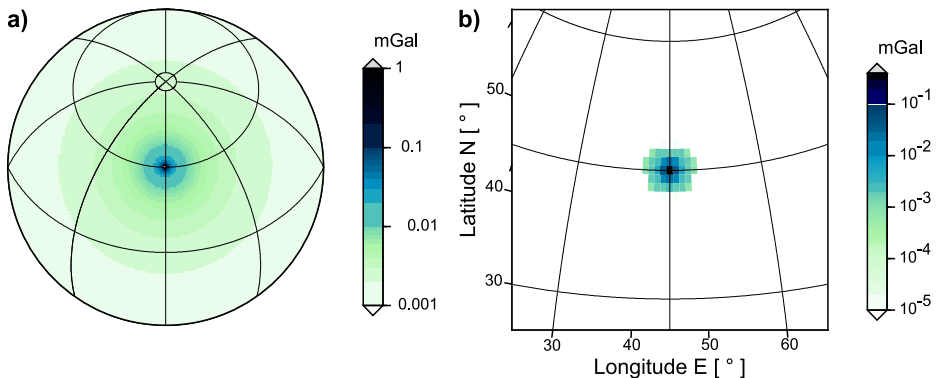


Fig. 13. The same as in Fig. 12, but for the gravity contribution.

References

- Chen C., Ren Z., Pan K., Tang J., Kalscheuer T., Maurer H., Sun Y. and Li Y., 2018. Exact solutions of the vertical gravitational anomaly for a polyhedral prism with vertical polynomial density contrast of arbitrary orders. *Geophys. J. Int.*, **214**, 2115–2132, DOI: 10.1093/gji/ggy250.
- D'Urso M.G., 2013. On the evaluation of the gravity effects of polyhedral bodies and a consistent treatment of related singularities. *J. Geodesy*, **87**, 239–252, DOI: 10.1007/s00190-012-0592-1.
- D'Urso M.G., 2014. Analytical computation of gravity effects for polyhedral bodies. *J. Geodesy*, **88**, 13–29, DOI: 10.1007/s00190-013-0664-x.
- Grombein T., Seitz K. and Heck B., 2013. Optimized formulas for the gravitational field of a tesseroid. *J. Geodesy*, **87**, 645–660, DOI: 10.1007/s00190-013-0636-1.
- Grombein T., Seitz K. and Heck B., 2014. Incorporating topographic-isostatic information into GOCE gravity gradient processing. In: Flechtner F., Sneeew N. and Schuh W.-D. (Eds), *Observation of the System Earth from Space - CHAMP, GRACE, GOCE and future missions: GEOTECHNOLOGIEN* Science Report No. 20. Springer, Berlin Heidelberg, 95–101, doi:10.1007/978-3-642-32135-1_12.

- Grüninger W., 1990. *Zur topographisch-isostatischen Reduktion der Schwere*. PhD Thesis. Universität Karlsruhe, Karlsruhe, Germany (in German).
- Hamayun, Prutkin I. and Tenzer R., 2009. The optimum expression for the gravitational potential of polyhedral bodies having a linearly varying density distribution. *J. Geodesy*, **83**, 1163–1170, DOI: 10.1007/s00190-009-0334-1.
- Heck B. and Seitz K., 2007. A comparison of the tesseroid, prism and point-mass approaches for mass reductions in gravity field modelling. *J. Geodesy*, **81**, 121–136, DOI: 10.1007/s00190-006-0094-0.
- Le Fehr T.R., 1991. An exact solution for the gravity curvature (Bullard B) correction. *Geophysics*, **56**, 1179–1184.
- Lin M. and Denker H., 2019. On the computation of gravitational effects for tesseroids with constant and linearly varying density. *J. Geodesy*, **93**, 723–747, DOI: 10.1007/s00190-018-1193-4.
- Mac Millan W.D., 1958. *Theoretical Mechanics. Vol. 2. The Theory of the Potential*. Dover, New York.
- Mader K., 1951. Das Newtonsche Raumpotential prismatischer Körper und seine Ableitungen bis zur dritten Ordnung. *Österreichische Zeitschrift für Vermessungswesen*, **11**, Special Issue.
- Marotta A.M. and Barzaghi R., 2017. A new methodology to compute the gravitational contribution of a spherical tesseroid based on the analytical solution of a sector of a spherical zonal band. *J. Geodesy*, **91**, 1207–1224, DOI: 10.1007/s00190-017-1018-x.
- Martinec Z., 1998. *Boundary-Value Problems for Gravimetric Determination of a Precise Geoid*. Lecture Notes in Earth Sciences, **73**. Springer, Berlin, Germany.
- Moritz H., 1980. *Advanced Physical Geodesy*. Herbert Wichmann Verlag, Karlsruhe, Germany.
- Nagy D., 1966. The gravitational attraction of a right rectangular prism. *Geophysics*, **31**, 362–371, DOI: 10.1190/1.1439779.
- Nagy D., Papp G. and Benedek J., 2000. The gravitational potential and its derivatives for the prism. *J. Geodesy*, **74**, 552–560, DOI: 10.1007/s001900000116.
- Nagy D., Papp G. and Benedek J., 2002. Corrections to The gravitational potential and its derivatives for the prism. *J. Geodesy*, **76**, 475, DOI: 10.1007/s00190-002-0264-7.
- Ren Z., Chen C., Pan K., Kalscheuer T., Maurer H. and Tang J., 2017. Gravity anomalies of arbitrary 3D polyhedral bodies with horizontal and vertical mass contrasts. *Surv. Geophys.*, **38**, 479–502, DOI: 10.1007/s10712-016-9395-x.
- Ren Z., Zhong Y., Chen C., Tang J., Kalscheuer T., Maurer H. and Li Y., 2018. Gravity gradient tensor of arbitrary 3D polyhedral bodies with up to third-order polynomial horizontal and vertical mass contrasts. *Surv. Geophys.*, **39**, 901–935, DOI: 10.1007/s10712-016-9395-x.
- Shen W.-B. and Deng X.-L., 2016. Evaluation of the fourth-order tesseroid formula and new combination approach to precisely determine gravitational potential. *Stud. Geophys. Geod.*, **60**, 583–607, DOI: 10.1007/s11200-016-0402-y.
- Torge W. and Müller J., 2012. *Geodesy*. 4th Edition. de Gruyter, Berlin, Germany.
- Tsoulis D., Jamet O., Verdun J. and Gonindard N., 2009. Recursive algorithms for the computation of the potential harmonic coefficients of a constant density polyhedron. *J. Geodesy*, **83**, 925–942, DOI: 10.1007/s00190-009-0310-9.
- Uieda L., Barbosa V. C. F. and Braatenberg C., 2015. Tesseroids: Forward-modeling gravitational fields in spherical coordinates. *Geophysics*, **81**(5), F41–F48, doi:10.1190/geo2015-0204.1.
- Vaníček P., Novák P. and Martinec Z., 2001. Geoid, topography, and the bouguer plate or shell. *J. Geodesy*, **75**, 210–215, DOI: 10.1007/s001900100165.

- Vaniček P., Tenzer R., Sjoberg L., Martinec Z. and Featherstone W., 2004. New views of the spherical bouguer gravity anomaly. *Geophys. J. Int.*, **159**, 460–472, DOI: 10.1111/j.1365-246X.2004.02435.x.
- Wessel P., Smith W.H.F., Scharroo R., Luis J.F. and Wobbe F., 2013. Generic Mapping Tools: Improved version released. *Eos Trans. AGU*, 409–410, DOI: 10.1002/2013EO450001.
- Wild-Pfeiffer F., 2008. A comparison of different mass elements for use in gravity gradiometry. *J. Geodesy*, **82**, 637–653, DOI: 10.1007/s00190-008-0219-8.
- Zhang Y. and Chen C., 2018. Forward calculation of gravity and its gradient using polyhedral representation of density interfaces: an application of spherical or ellipsoidal topographic gravity effect. *J. Geodesy*, **92**, 205–218, DOI: 10.1007/s00190-017-1057-3.